

Decolorization of malachite green in aqueous solution via MgO nanopowder

H. Idriss^{a, b*}

^a*Department of Physics, College of Science, Imam Mohammad Ibn Saud Islamic University (IMSIU), P.O.Box 90950, Riyadh 11623, Saudi Arabia*

^a*Deanship of Scientific research, Imam Mohammad Ibn Saud Islamic University (IMSIU), Saudi Arabia.*

Water is one of the essential primary resources for life and development on the planet, where many industrial activities depend on it, but some industries lead to water pollution. Hence, we need economical and effective ways to address the contamination. This article describes the production and utilization of MgO nanopowder using thermal decomposition as an economical and efficient method for malachite green decolorization. The MgO nanopowder was analyzed via various techniques for morphology, cryptography, surface area, etc. Batch adsorption tests have been performed as a function of contact time, pH, and initial dye concentration to study their impact on decolorization of malachite green via MgO nanopowder. The result verified the target nanopowder's production with crystallite size 20.16 nm and a relative surface area of 19.84 m² /g. MgO nanopowder was employed to decolorize malachite green dye in an aquatic solution utilizing a batch method. The findings revealed that the maximum adsorption capacity value was 232.26 mg/g. The adsorption was found to follow the Freundlich isotherm models and follow the pseudo-second-order kinetics.

(Received September 25, 2021; Accepted December 4, 2021)

Keywords: MgO, nanopowder, synthesis, isotherm, Kinetics, Adsorption

1. Introduction

Water pollution has become a dangerous issue in this age of the fast increase in community, civilization, the industrial revolution, climate change (Islam, et al.,2019). Dyes are a sort of contaminants that can presents in wastewater due to the industries activities, including stoneware, pigment, variegation, cosmetics, and textile (Dastgerdi et al.,2019). The demand for dye application has been increased by greater than 1000 tons/year. About 10–15% of these are emancipated into drainage and sewerage throughout the dyeing process 15% of the dye waste is emancipated into the waste streams as liquid waste during the coloring operation (Adegoke and Bello.,2015). Numerous adsorbents materials have been examined for their applicability in the dye treatment in aqueous solution (Palma et al.,2016; Salama, 2017; Maleki et al.,2018). Biological process in wastewater treatment is slow and inefficient on organic dyestuff contaminants; whereas chemical and pPhysical methods and techniques are more effective(Daneshvar et al.,2006; Sathian et al.,2014; Su et al.,2016; Cruz-Rizo et al.,2017; Siyal et al.,2020). Nanotechnology has earned considerable application as an effective separation method in dyes detoxification (Zhang et al.,2013; Dhal et al.,2015; Dil et al.,2015; Nguyen et al.,2019). However, the metal oxide nanoparticles have an immense interest because of their unique stability and electro-catalytic activity(Huang et al.,2010). Metal oxides nanopowder has various environmental, optics, medical, sensor, and advanced utilization depends on their chemical and physical characteristics (Xu, et al.,2016; Ogunsonaetal., 2019; Khaleel et al.,2019). Among these nanomaterials, the MgO nanoparticle is widely investigated due to its noble characteristic, ease of synthesis, and low cost(Mahmoud et al., 2016; Xu et al.,2018;). Malachite green (MG) is an organic dye widely used in food, industry, textile, and pesticide in aquatic environments (Nethaji et al.,2010). It is reported that the malachite green has toxicity even at a few levels of 1 mg/l. MG has carcinogenic attributes

* Corresponding author: hjoidriss@gmail.com

and potential genetic effects for humans, so it was banned earlier in Europe because of the fish consumption of MG dye that causes potential exposure to the user (Arumugam et al.,2019). In this article, MgO nanopowder has been synthesized and characterized as fast adsorbent materials for the decolorizing malachite green in aquatic media using the thermal decomposition method.

2. Experimental

2.1. Fabrication of MgO nanopowder

MgCO₃ was gained from Sigma Aldrich and used as a precursor in the absence of any chemical purification to obtain MgO nanopowder. A weight of 4.5g MgCO₃ was put into a ceramic crucible inside the oven under ambient circumstances for thermal decomposition at 700 oC for 3 hours; afterword, the MgO nanopowder was acquired.

2.2. Characterization of MgO nanopowder

MgO was examined using X-ray diffraction (XRD) (Bruker, Germany). A scanning electron microscope (Phenom XL, Netherland) was employed for morphological and elemental studies. The specific surface area of MgO nanopowder was estimated via N₂ adsorption-desorption isotherms using ASAP 2020 Micro metrics apparatus.

2.3. Adsorption equilibrium test

MG dye stock solution (500 ppm) was prepared using distilled water and stored in the dark at room temperature. The adsorption equilibrium was achieved in 50 ml glass beakers contain 0.05 g of MgO nanopowder. Subsequently, 10 ml of MG with concentrations 50, 100, 200, 300, 400, and 500 ppm were added to 0.05 g of MgO at room temperature and stirred using a shaker (250 rpm) for 60 min, and PH 3 kept constant. The beaker's contents were isolated using filter paper (3000 rpm). After the test finished, the solution was extracted from the adsorbent using filter paper and measured using the UV - Vis spectrophotometer at 620 nm. The amount of MG adsorbed by an adsorbent at a time) qt) was computed using equation(1).

$$q_t = \frac{V(C_0 - C_t)}{m} \quad (1)$$

where, q_t (mg g⁻¹) is mass of dye adsorbed by a unit mass of nanopowder m (g) at time t (min), V is the solution volume (L), C_0 concentration of the dye initially preset and C_t is that at t time in (mg L⁻¹). On the other hand, the removal percentage (%)of the dye by adsorption at time(t) can be calculated by formula (2).

$$removal(\%) = \frac{(C_0 - C_t)}{C_0} \times 100 \quad (2)$$

2.4. Adsorption kinetic test

The adsorption kinetic study was performed using MgO (0.05g) and 200 ppm MG concentration mixed together in 50ml beakers and stirred using shaker (250 rpm).The solution was extracted from the adsorbent using filter paper at a different times 10,20,30,40,50 and 60 min and measured using the UV - Vis spectrophotometer at 620 nm. The amount of MG adsorbed by adsorbent at equilibrium (q_e) was computed using equation(3)

At equilibrium, an analogous formula is employed to find out the mass adsorbed q_e :

$$q_e = \frac{V(C_0 - C_e)}{m} \quad (3)$$

2.5. Adsorption isotherm theory

To determine the absorption capacity of sorbents for the removal of MG dyes, the most commonly used isotherm, Freundlich and Langmuir have been chosen.

$$\frac{C_e}{q_e} = \frac{1}{q_m} C_e + \frac{1}{q_m \cdot K_L} \quad \text{Langmuir (linear equation)} \quad (4)$$

$$\ln q_e = \frac{1}{n} \ln C_e + \ln K_F \quad \text{Freundlich linear (equation)} \quad (5)$$

C_e = the equilibrium concentration of adsorbate (mg/L-1) q_e = the amount of dye adsorbed per gram of the adsorbent at equilibrium (mg/g), q_m = maximum monolayer coverage capacity (mg/g) K_L = Langmuir isotherm constant (L/mg). q_m and K_L represent the slope and intercept of C_e/q_e versus C_e plotting. Whereas, k and n of Freundlich equation are taken from the $\ln q_e$ versus $\ln C_e$ diagram. K_F and n of the Freundlich model are associated with the adsorptive bond strength and distribution, sequentially. To express the compatibility between experimental data and kinetic models, the value of the correlation coefficient (R^2) was used. Equation (6) describes a pseudo-first-order model having a rate constant k_1 ($\text{l} \cdot \text{min}^{-1}$). From the slope and intercept of $\ln(q_e - q_t)$ versus t plot, k_1 and q_e can respectively be determined.

$$\ln(q_e - q_t) = \ln(q_e) - k_1 \cdot t \quad (6)$$

A pseudo-second-order is modeled by equation (7), where k_2 denotes the rate constant ($\text{g} \cdot \text{mg}^{-1} \cdot \text{min}^{-1}$). Using of t/q_t against t graph, q_e and k_2 are correspondingly obtained from the slope and intercept.

$$\frac{t}{q_t} = \frac{1}{k_2 \cdot q_e^2} + \frac{t}{q_e} \quad (7)$$

3. Result and discussion

3.1. XRD study of the MgO nanopowder

The XRD pattern of MgO nanopowder is displayed in Fig (1).

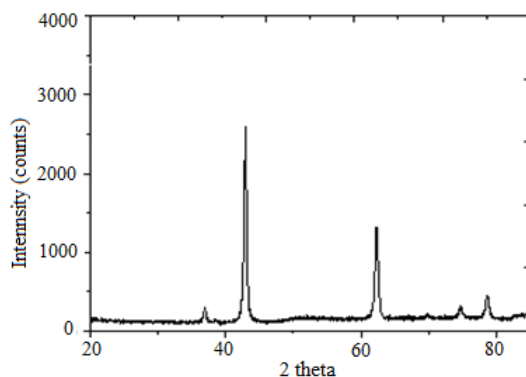


Fig. 1. XRD pattern of MgO nanopowder.

The spectra exhibit good crystallinity for a hexagonal phase of MgO nanopowder. The highest peaks region (2θ) of MgO nanopowder was at 42.9236. The diffraction peaks might be recorded to the face-centered cubic structure of MgO (JCPDS card No: 78-0430). No characteristics peaks of impurities were identified in the XRD pattern. Significantly expanded lines in the XRD pattern indicated that nanoparticles' presence in the samples (Modwi et al.,2018). The XRD pattern is employed for achieving the average crystallite size with the aid of Debye - Scherer's equation (8).

$$D = \frac{0.9\lambda}{\beta \cos \theta} \quad (8)$$

(where: D , λ , β and θ are the crystallite size, the wavelength of the X-ray source (Cu $K\alpha$), full width at half maximum (FWHM) and Bragg's diffraction angle respectively). The average crystallite size of the synthetic MgO nanopowder was found to be 20.16 nm.

3.2. Study of the morphological and elemental content of MgO nanopowder

The surface morphology of MgO nanopowder in different magnification are presented in fig (2). The surface shape tends to the coffee beans at magnification 100 micro when the magnification has increased the shape. When the magnification increases, the shape becomes closer to the regular mushroom pieces. The EDX revealed that no impurities were identified in the MgO nanopowder sample, as shown in fig2.

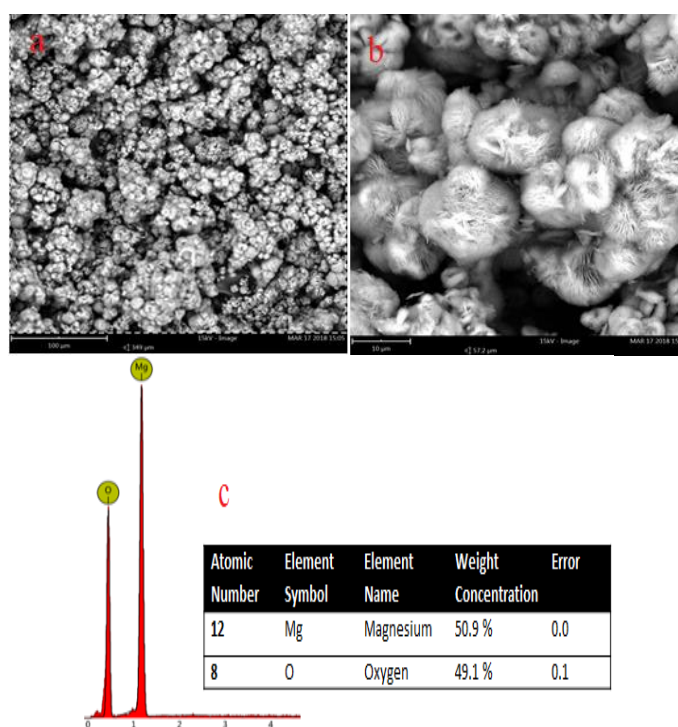


Fig. 2. Morphological and elemental evaluation of MgO nanopowder and elemental contents.

3.3. Determination of the specific surface area of MgO nanopowder

MgO nanopowder specific surface area computed from the N₂ adsorption/desorption isotherms, which were achieved using an automated surface area analyzer ASAP 2020 Micro metrics apparatus. The specific surface area was obtained from the BET method and found to be \approx 19.84 m²/g. 20.16 nm

3.4. Effect of initial dye concentration on decolorization

Figure (3) presents the percentage removal of MG dye via MgO nanopowder in an aqueous solution. When the concentration increases, the removal percentage decreases gradually because of the adsorption capacity limitation of the adsorbent. Although the removal percentage is very high in all concentrations studied, however in the low concentration, the percentage of removal is very high compared with the high concentrations. On the other hand, this means that a certain mass of MgO nanopowder can only absorb a fixed amount of the MG dye. This might be associated with an increment in the concentration gradient's driving force with increased initial MG concentration (Agarwal et al.,2016). The highest removal percentage recorded was 99.996 %, and the lowest removal percentage was 99.992 %. This implies that the MgO nanopowder has strong characteristics in MG removal.

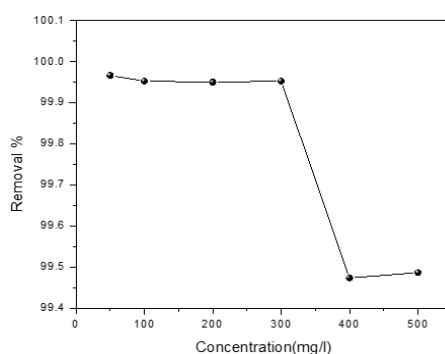


Fig. 3. Effect of initial dye concentration on removal efficiency.

3.5. Effect of contact time on decolorization

To examine the effect of contact time on MG dye adsorption onto MgO nanopowder, 200 ppm solution of MG with pH of 3 was computed. The experiments were performed at various times (10-60 minutes), and after each time, one sample was taken directly, filtered, and analyzed. Figure (4) display the dye percentage removal as a function of contact times.

Obviously, The percentage removal of MG increases with time increase. About 85% of MG dye removal occurred around 10 min. Of course, this might be attributed to the presence of free active sites on the surface of MgO nanopowder; however, it becomes saturated after a period of time (Agarwal et al.,2016). the Adsorption process equilibrium was accomplished near 40 minutes at this stage, about 99.8 % of MG dye removal occurred. Thus, the equilibrium time to absorb the dye from aqueous solutions is about 40 min of contact time. The optimum contact time to absorb the MG dye from aquatic solutions is 10 min.

3.6. Effect of contact time on removal efficiency

To examine the effect of contact time on MG dye adsorption onto MgO nanopowder 200 ppm solution of MG with pH of 3 was computed. The experiments were performed at various time (10-60 minutes) and after each time, one sample was taken directly filtered and analyzed. Figure (4) display the dye percentage removal as function of contact times. Obviously, The percentage removal of MG increases with time increase. about 85% of MG dye removal occurred around 10 min. Of course this might be attributed to the presence of amount of free active sites on the surface of MgO nanopowder however after a period of time it becomes saturated (Agarwal et al.,2016). the Adsorption process equilibrium was accomplished near 40 minutes at this stage about 99.8 % of MG dye removal occurred. Thus, the equilibrium time to absorb the dye from aqueous solutions is about 40 min of contact time, and the optimum contact time to absorb the MG dye from aquatic solutions is 10 min.

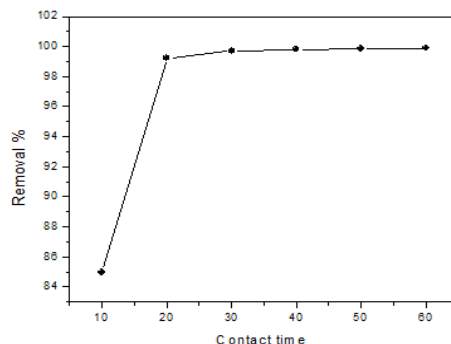


Fig. 4. Effect of contact time on removal efficiency.

3.6. Effect of pH on decolorization

One of the essential circumstances that regulate MG adsorption on the absorbent material is the solution's pH. Thus, an increase in pH value may produce a rise or dwindling in the adsorption capacity (Amin,2009). To study the effect of pH on MG's removal efficiency by MgO nanopowder, the experiment was conducted at 200 ppm MG dye concentration with a 0.05 g mass of MgO nanopowder for 60 min equilibrium time. Figure (5) shows the percentage removal of MG dye via MgO nanopowder in various PH (2.6, 5.6, 7.6, 8.6, 9.6,11.6). From the figure, it is observed that percentage removal of MG increase with pH increases. The lower removal percentage rate of MG dye by MgO nanopowder was 61.05%, and the highest was 99.95%. When the pH values rise, the surface of the sorbent material is negatively charged, and the absorption of the dye molecules increases due to the electrical attraction between the surface and cationic dye molecules. On the other hand, at low pH values, the sorbent material's surface will be charged positively. The expected trend is to reduce dye absorption due to electrostatic repulsion between the positive dye molecules and the surface of the absorbent material (Tang et al.,2019).

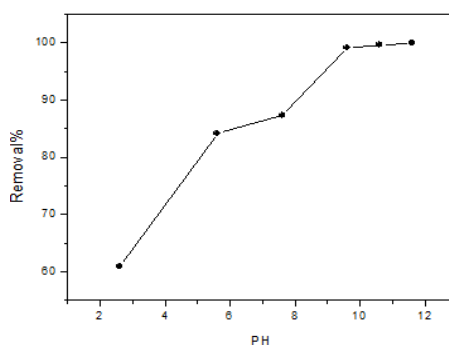


Fig. 5. Effect of pH on removal efficiency.

3.7. Adsorption isotherm

An adsorption isotherm model is an explanation of the relationship between the quantity of solute adsorbed and the concentration of the solute in the aqueous phase since the adsorption isotherms are essential to explain how adsorbates will interact with the adsorbents and thus are important for design objectives; hence, the correlation of equilibrium data using the model is crucial for working adsorption process (Salam et al.,2011) In this work, two models Langmuir and Freundlich's isotherms have been applied. Figures 6 and 7 exhibit the linearized Langmuir adsorption and Freundlich isotherms for MG dye removal via MgO nanopowder at room temperature, respectively. The information regarding the Langmuir isotherms parameters was computed through the least square's method Table (1) presents the Langmuir and Freundlich isotherms parameters for adsorption of MG dye by MgO nanoparticles. From table (1), the

Langmuir isotherm constant revealed that the value of (q_m) was found to be 233.26 mg/g. Moreover, the Langmuir isotherm constant can be explained by the equilibrium parameter (separation factor R_L), which is a constant without dimensions described in formula 9 (Ho et al.,2002).

$$R_L = \frac{1}{1 + k_l \times C_0} \quad (9)$$

Table 1. Adsorption equilibrium constants for the dye removal by MgO nanopowder.

| Langmuir constants | | | | Freundlich constants | | |
|------------------------------------|------------------------------------|--------|--------|----------------------|---------|--------|
| $q_m(\text{mg}\cdot\text{g}^{-1})$ | $K_L(\text{l}\cdot\text{mg}^{-1})$ | R_L | r^2 | n | k_f | r^2 |
| 232.26 | 17.2459 | 0.0001 | 0.7184 | 1.1824 | 1614.82 | 0.9925 |

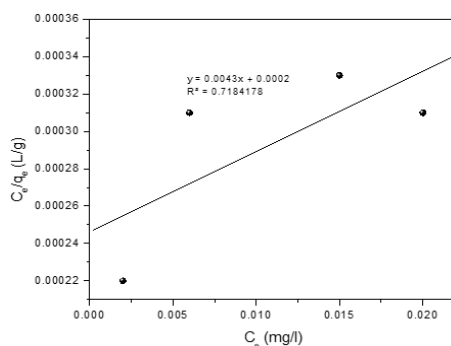


Fig. 6. Plot of linearized Langmuir adsorption isotherm.

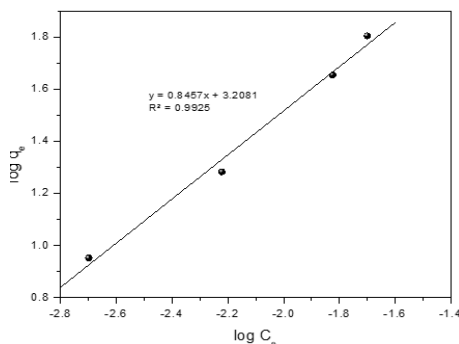


Fig. 7. Plot of linearized Freundlich adsorption isotherm.

The magnitude of R_L fall between 0 and 1 this implies that the adsorption is favorable for all the initial dye concentration. On the other hand, the magnitude of the Freundlich isotherm constant (n) indicates the adsorption intensity. The magnitude of n was between 1 and 10; this confirms the favorable condition for the adsorption. The two models describe the correlation coefficient (R^2). From the obtained values of (R^2), the adsorption was found to obey the Freundlich isotherms R^2 (0.9925). Although, numerous sorbents have been utilized for MG dye decolorization from the aqueous solution. However, the MgO nanopowder used in this study has a very high absorption capacity compared with other reported adsorbents, as presented in table (2).

Table 2. A summary of the comparison between the values of the adsorption capacity of MgO nanopowder with other reported adsorbents.

| adsorbent | Adsorption capacity (mg/g) | Reference |
|------------------------------------|----------------------------|------------------------------|
| MgO nanopowder | 232.26 | Current study |
| Metal–Organic Frame workMIL-53(Al) | 164.9 | (Lin and Chang,2015) |
| Multi-walled carbon nanotube | 80.64 | (Ghaedi etal.,2016) |
| Halloysite nanotubes | 99.6 | (Kiani etal.,2011) |
| Activated carbon | 27.78 | (Santhi etal.,2010) |
| Oil palm trunk fibre | 149.35 | (Hameed and El-Khaiary,2008) |
| Rubber wood | 36.46 | (Kumar and Sivanesan 2007). |
| Jute fiber carbon | 136.58 | (Porkodi and Kumar,2007) |
| Bagasse fly ash | 170.33 | (Mall,2005) |
| Ultrathin NiO nanoflakes | 142.08 | (Wei,2014) |

3.8. Adsorption kinetics

The kinetics of MG dye adsorption via MgO nanopowder was investigated concerning various initial concentrations. To estimate the Pseudo first order, the pseudo-second-order was employed to fit the experimental data using the linear regression analysis method. The parameters of this model are gathered in Table (3). High correlation coefficient magnitudes (R^2) indicate the suitability of the order of the kinetic model. Figure (8) shows the pseudo-first-order kinetic model, and figure (9) presents the pseudo-second-order kinetic model for MG dye removal by MgO nanopowder at room temperature. From the figures, the correlation coefficient (R^2) is high for the pseudo-second-order kinetic model than the pseudo-first-order kinetic model. Therefore, the adsorption of MG dye via MgO nanopowder is obeyed the pseudo-second-order kinetic model. The kinetic data information, the (Q_E) value computed from the pseudo-first-order is less than the experimental value. Nevertheless, the calculated (Q_E) value from the pseudo-second-order is almost closed to the experimental value.

Table 3. Pseudo-Second order kinetic parameters for the dye adsorption by MgO nanoparticles.

| $q_{m(\text{exp})}^a$ (mg.g^{-1}) | First-order | | r^2 | r^2 | Second-order | | r^2 | |
|---|--|---|-------|--------|---|---|-------|--------|
| | $k_1 \times 10^2$ (L.g^{-1}) | $q_{m(\text{cal})}^b$ (mg.g^{-1}) | | | k_2 ($\text{mg.g}^{-1} \cdot \text{L.g}^{-1}$) | $q_{m(\text{cal})}^b$ (mg.g^{-1}) | | |
| 59 | | 0.0319 | 5.73 | 0.7314 | | 0.0446 | 59.43 | 0.9992 |

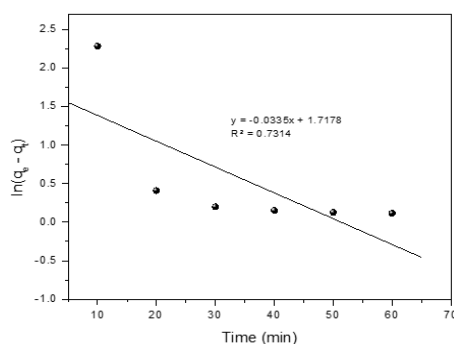


Fig. 8. Pseudo-first-order kinetic model for MG dye removal by MgO nanopowder.

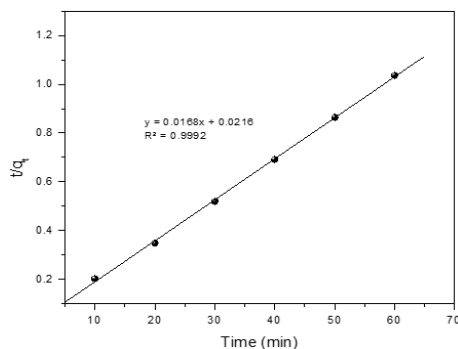


Fig. 9. Pseudo-first-order kinetic model for MG dye removal by MgO nanopowder.

4. Conclusion

Based on the outcomes, we conclude that the thermal decomposition method for MgO nanopowder production is the easiest and economical, and eco-friendly method. The current study shows that MgO nanopowder is an effective sorbent for the decolorization of malachite green in an aqueous solution. The maximum capacity of sorbent was found to be 232.26 mg/g. The adsorption of malachite green in the aquatic system by MgO nanopowder is obeyed the pseudo-second-order kinetic model

References

- [1] K. A. Adegoke, O. S. Bello, *Water Resources and Industry* **12**, 8 (2015).
- [2] S. Agarwal, I. Tyagi, V. K. Gupta, S. Mashhadi, M. Ghasemi, *Journal of Molecular Liquids* **223**, 1340 (2016).
- [3] S. Agarwal, I. Tyagi, V. K. Gupta, S. Mashhadi, M. Ghasemi, *Journal of Molecular Liquids* **223**, 1340 (2016).
- [4] N. K. Amin, *Journal of hazardous materials* **165**(1-3), 52 (2009).
- [5] T. K. Arumugam, P. Krishnamoorthy, N. R. Rajagopalan, S. Nanthini, D. Vasudevan, *International journal of biological macromolecules* **128**, 655 (2019).
- [6] A. Cruz-Rizo, S. Gutiérrez-Granados, R. Salazar, J. M. Peralta-Hernández, *Separation and Purification Technology* **172**, 296 (2017).
- [7] N. Daneshvar, M. Ayazloo, A. R. Khataee, M. Pourhassan, *Bioresource technology* **98**(6), 1176–1177 (2007).
- [8] Z. H. Dastgerdi, V. Abkhiz, S. S. Meshkat, N. Ghorbani, *Journal of Environmental Chemical Engineering* **7**(3), 103109 (2019).
- [9] J. P. Dhal, M. Sethi, B. G. Mishra, G. Hota, *Materials Letters* **141**, 267 (2015).
- [10] E. A. Dil, M. Ghaedi, A. Asfaram, S. Hajati, F. Mehrabi, A. Goudarzi, *Ultrasonics Sonochemistry* **34**, 677 (2017).
- [11] M. Ghaedi, K. Dashtian, A. M. Ghaedi, N. Dehghanian, *Physical Chemistry Chemical Physics* **18**(19), 13310 (2016).
- [12] B. H. Hameed, M. I. El-Khaiary, *Journal of hazardous materials* **154**(1-3), 237 (2008).
- [13] Y. S. Ho, C. T. Huang, H. W. Huang, *Process Biochemistry* **37**(12), 1421 (2002).
- [14] S. Y. Huang, P. Ganesan, B. N. Popov, *Applied Catalysis B: Environmental* **96**(1-2), 224–230 (2010).
- [15] M. A. Islam, I. Ali, S. A. Karim, M. S. H. Firoz, A. N. Chowdhury, D. W. Morton, M. J. Angove, *Journal of Water Process Engineering* **32**, 100911 (2019).
- [16] W. A. Khaleel, S. A. Sadeq, I. A. M. Alani, M. H. M. Ahmed, *Optics & Laser Technology* **115**, 331 (2019).
- [17] G. Kiani, M. Dostali, A. Rostami, A. R. Khataee, *Applied Clay Science* **54**(1), 34 (2011).
- [18] K. V. Kumar, S. Sivanesan, *Dyes and Pigments* **72**(1), 124 (2007).

- [19] K. Y. A. Lin, H. A. Chang, *Chemosphere* **139**, 624 (2015).
- [20] H. R. Mahmoud, S. M. Ibrahim, S. A. El-Molla, *Advanced Powder Technology* **27**(1), 223016).
- [21] A. Maleki, M. Mohammad, Z. Emdadi, N. Asim, M. Azizi, J. Safaei, *Arabian Journal of Chemistry* (2018).
- [22] I. D. Mall, V. C. Srivastava, N. K. Agarwal, I. M. Mishra, *Colloids and Surfaces A: Physicochemical and Engineering Aspects* **264**(1-3), 17 (2005).
- [23] A. Modwi, L. Khezami, K. K. Taha, H. Idriss, *Zeitschrift für Naturforschung A* **73**(11), 975018).
- [24] S. Nethaji, A. Sivasamy, G. Thennarasu, S. Saravanan, *Journal of Hazardous Materials* **181**(1-3), 271 (2010).
- [25] C. H. Nguyen, R. S. Juang, *Journal of the Taiwan Institute of Chemical Engineers* **99**, 166019).
- [26] E. O. Ogunsona, R. Muthuraj, E. Ojogbo, O. Valero, T. H. Mekonnen, *Applied Materials Today*, 100473 (2019).
- [27] C. Palma, L. Lloret, A. Puen, M. Tobar, E. Contreras, *Chinese Journal of Chemical Engineering* **24**(4), 521 (2016).
- [28] K. Porkodi, K. V. Kumar, *Journal of hazardous materials* **143**(1-2), 311 (2007).
- [29] O. E. A. Salam, N. A. Reiad, M. M. ElShafei, *Journal of Advanced Research* **2**(4), 297011).
- [30] A. Salama, *Journal of colloid and interface science* **487**, 348 (2017).
- [31] T. Santhi, S. Manonmani, T. Smitha, *Journal of hazardous materials* **179**(1-3), 178 (2010).
- [32] S. Sathian, M. Rajasimman, C. S. Rathnasabapathy, C. Karthikeyan, *Journal of Water Process Engineering* **4**, 82 (2014).
- [33] A. A. Siyal, M. R. Shamsuddin, A. Low, N. E. Rabat, *Journal of environmental management* **254**, 109797 (2020).
- [34] C. X. H. Su, L. W. Low, T. T. Teng, Y. S. Wong, *Journal of Environmental Chemical Engineering* **4**(3), 3618 (2016).
- [35] S. Tang, D. Xia, Y. Yao, T. Chen, J. Sun, Y. Yin, Y. Peng, *Journal of colloid and interface science* **554**, 682 (2019).
- [36] T. Tolaymat, A. El Badawy, A. Genaidy, W. Abdelraheem, R. Sequeira, *Journal of cleaner production* **143**, 401 (2017).
- [37] A. Wei, B. Liu, H. Zhao, Y. Chen, W. Wang, Y. Ma, S. Liu, *Chemical Engineering Journal* **239**, 141 (2014).
- [38] J. Xu, P. Wu, E. C. Ye, B. F. Yuan, Y. Q. Feng, *TrAC Trends in Analytical Chemistry* **80**, 41 (2016).
- [39] J. Xu, D. Xu, B. Zhu, B. Cheng, C. Jiang, *Applied Surface Science* **435**, 1136 (2018).
- [40] Y. R. Zhang, S. Q. Wang, S. L. Shen, B. X. Zhao, *Chemical engineering journal* **233**, 258 (2013).